Effects of Nose Bluntness, Angle of Attack, and Oscillation Amplitude on Hypersonic Unsteady Aerodynamics of Slender Cones

LARS ERIC ERICSSON*
Lockheed Missiles & Space Company, Sunnyvale, Calif.

A previously developed analytic theory for the unsteady aerodynamics of moderately blunt slender cones has been extended to include the effects of large nose bluntness, nonzero angles of attack, and finite oscillation amplitudes. It is shown that the developed theory agrees well with available experimental data and correctly predicts the opposite effects of nose bluntness on static and dynamic stability including the highly nonlinear characteristics at angles of attack and oscillation amplitudes up to cone half-angle magnitudes. A universal scaling law has been derived that gives the nose-bluntness effects on static and dynamic characteristics for the above angle-of-attack and amplitude ranges with sufficient accuracy for preliminary design of conical re-entry vehicles flying ballistic or lifting re-entry trajectories.

Nomenclature

a = speed of sound, m/sec
A_1,A_2 = constants defining f^*, Eq. (6)
ΔA = surface area element, m²
c = reference length, m (cone base diameter, d_B)
d_B = base diameter, m
d_N = nose (bluntness) diameter, m
D_N = nose drag; coefficient $C_{D_N} = D_N/(\rho_\infty U_\infty^2/2)(\pi d_N^2/4)$
F = pressure correlation function
f^* = dynamic pressure ratio, $f^* = \rho U^2/\rho_\infty U_\infty^2$
g^* = velocity ratio, $g^* = U/U_\infty$
j = blast wave pressure correlation function
$k(\gamma)$ = shock parameter defined in Eq. (9)
l = sharp cone body length, m (see inset in Fig. 4a)
M = Mach number, $M = U/a$
M_p = pitching moment, kgm; coefficient $C_m = M_p/(\rho_\infty U_\infty^2/2)Sc$
M,N = number of terms in sum—representation of integrals defining effective stability derivatives, Eqs. (33) and (36)
p = static pressure, kg/m²; coefficient $C_p = (p - p_\infty)/(\rho_\infty U_\infty^2/2)$
p_0 = blast wave pressure, kg/m²; coefficient $C_{p_0} = (p_0 - p_\infty)/(\rho_\infty U_\infty^2/2)$
q = rigid body pitch rate, rad/sec
r = body radius, m (see Fig. 1)
R = radial distance from bow shock centerline, m (see Fig. 1)
R_{sh} = bow shock radius, m (see Fig. 1)
R_{l_∞} = Reynolds number, $R_{l_\infty} = lU_\infty/\nu_\infty$
S = reference area, m², $S = \pi c^2/4$
t,T = time and oscillation period, sec
U = axial velocity, m/sec
$V_\perp$ = velocity normal to body surface, m/sec
x = axial coordinate, m (see Fig. 1)
x_0 = centroid location of equivalent sphere representing blunt nose, m; $x_0 = 0$ for spherical nose bluntness
$\Delta\bar{x}$ = cone center of gravity location forward of base, m
z = translatory coordinate, m (see Fig. 1)
α = angle of attack, rad or deg
α_0 = trim angle of attack, rad or deg
β = angular body coordinate, rad or deg (see Fig. 1)
γ = ratio of specific heats ($\gamma = 1.4$ for air)
Δ = difference or increment
θ = body perturbation in pitch, rad or deg
θ_c = cone half-angle, rad or deg
θ_F = surface slope, rad or deg (see Fig. 1)
Λ = nose-bluntness parameter defined in Eq. (9)
ν = kinematic viscosity of air, m²/sec
ρ = air density, kg-sec²/m⁴
ϕ = azimuth location, rad or deg (see Fig. 1)
χ,χ^*,χ^{**} = hypersonic similarity parameters defined in Eqs. (8) and (14)
$\bar{\chi}_l,\chi_l$ = hypersonic scaling parameters defined in Eqs. (39) and (40)
ψ = phase angle, rad, $\psi = \omega t$
ω = pitch frequency, rad/sec

Subscripts

B = base
c = cone
c.g. = center of gravity or oscillation center
inst = instantaneous
L = local
max = maximum
min = minimum
n = numbering subscript
N = nose
Newt = Newtonian value
sh = bow shock
∞ = freestream conditions

Superscripts

i = induced—e.g., $\Delta^i C_p$ = nose bluntness induced pressure (change) on aft body
= values behind a normal shock, e.g., $\hat{p}$

Derivative symbols

$\dot{\theta}$ = $\partial\theta/\partial t$
C_{m_q} = $\partial C_m/\partial(cq/U_\infty)$; $C_{m_{\dot{\alpha}}} = \partial C_m/\partial(c\dot{\alpha}/U_\infty)$
C_{m_α} = $\partial C_m/\partial\alpha$; $C_{m_\theta} = \partial C_m/\partial\theta$
$C_{m_{\dot{\theta}}}$ = $C_{m_q} + C_{m_{\dot{\alpha}}}$
$C_{\bar{m}_\theta},C_{\bar{m}_{\dot{\theta}}}$ = effective derivatives defined in Eqs. (31) and (32)

Presented as Paper 70-216 at the AIAA 8th Aerospace Sciences Meeting, New York, January 19–21, 1970; submitted February 27, 1970; revision received June 10, 1970. This work was supported by the LMSC Independent Development Program.

* Senior Staff Engineer. Associate Fellow AIAA.

Introduction

IT has long been recognized that nose bluntness can have large effects on aft body loads at hypersonic speeds. These effects have been observed on cylinder-flare bodies as

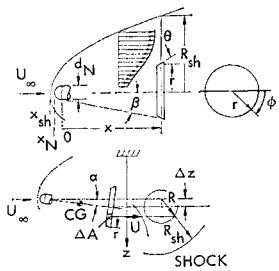

Fig. 1 Shock-induced inviscid shear flow at near zero angle of attack.

well as on blunted slender cones. Analytic and numerical methods have been developed that in most cases satisfactorily describe the static vehicle characteristics. However, none of the presently available theories known to the author offers a realistic description of the unsteady characteristics, manifested by the poor correlation between theory and experiment that is obtained when the nose-bluntness-induced effects are not small.

A new theory is described that provides a realistic mathematical model of the nose-bluntness-induced effects on unsteady aerodynamics. The theory has the following features: 1) It is analytic and hence simpler than most theories presently in use. 2) It gives a breakdown of the unsteady aerodynamic characteristics into local and nose-bluntness-induced components and, therefore, is a useful preliminary design tool. 3) It can use experimental static data as an input and can thereby include some of the viscous flow effects.

Analytic Approach

The inviscid shear flow over the aft body is determined by the shape of the bow shock.[1–5] The shock shape is essentially determined by the nose bluntness and can be related to the nose drag.[6] Thus the inviscid shear flow can be determined relatively simply. The embedded-Newtonian flow concept[4] can be used to determine the forces on a body element embedded in the entropy wake generated by the nose (Fig. 1).

Since the shock shape is rather insensitive to the attitude of a blunt nose, hemispherical or blunter, there are only two mechanisms for changing the aerodynamic force on the body element: 1) through local crossflow change; 2) through translation of the body element in the inviscid shear flow profile.

In the steady case, it does not matter whether the translation of the body element occurs through movement of the body element or through movement of the blast wave center, i.e., the nose. In the unsteady case, however, a time lag occurs in the latter case before a translatory movement of the nose has resulted in translation of the inviscid shear flow profile at the body element. The neglect of this time lag, inherent in existing theories known to the author, causes the poor correlation between theory and dynamic test data for blunted slender cones.

Basic Equations

Using the embedded-Newtonian flow concept,[4] the pressure coefficient on the body element in Fig. 1 can be written

$$C_p = C_{p_0} + C_{p_{\text{Newt}}} \rho U^2/\rho_\infty U_\infty^2$$

$$C_{p_{\text{Newt}}} = C_{p_{\max}}(V_\perp/U)^2 \tag{1}$$

where $C_{p_{\max}}$ is well approximated by the stagnation pressure behind a normal shock ($C_{p_{\max}} \approx 1.8$) for blunt bodies and by the Newtonian value ($C_{p_{\max}} \approx 2$) for slender geometries. $V_\perp$ is the local velocity component normal to the surface of the body element, and U is the local axial velocity component in the inviscid shear flow. That is, $V_\perp/U$ is determined geometrically and, for the body element in Fig. 1 pitching at the rate of q rad/sec, it is

$$V_\perp/U = \cos\alpha \sin\theta_F + \sin\alpha \cos\theta_F \sin\phi + [(x - x_{CG} + r \tan\theta_F)q/U] \cos\theta_F \sin\phi \tag{2}$$

The dynamic pressure ratio is a function of radial position in the inviscid shear flow profile. If similar profiles are assumed,† it can be expressed in the following form:

$$\rho U^2/\rho_\infty U_\infty^2 = f^*(R/R_{sh}) \tag{3}$$

R_{sh} is determined by the nose drag[6]:

$$R_{sh}/d_N \approx 1.0 C_{D_N}^{1/4}(x/d_N - x_{sh}/d_N)^{1/2} \tag{4}$$

where $x_{sh} = x_N$.

R is obtained from Fig. 1

$$\left(\frac{R}{d_N}\right)^2 = \left(\frac{\Delta z}{d_N}\right)^2 + 2\frac{\Delta z}{d_N}\cos\alpha\left(\frac{1}{2} + \frac{x}{d_N}\tan\beta\right)\sin\phi + \left(\frac{1}{2} + \frac{x}{d_N}\tan\beta\right)^2 [\cos^2\alpha \sin^2\phi + \cos^2\phi] \tag{5}$$

(α and β defined in Fig. 1).

In Eq. (3), $f^*(R/R_{sh})$ is of parabolic shape and can be represented[7] as

$$f^*(R/R_{sh}) = f_0 + A_1\chi^* + A_2\chi^{*2} \tag{6}$$

where

$$\chi^* = (R/d_N - \tfrac{1}{2})^2/(R_{sh}/d_N)^2$$

and f_0 is closely approximated by the (R_{sh}/d_N) pressure ratio through a normal shock. Seiff's data[3,7] for a spherically blunted cylinder give

$$\rho U^2/\rho_\infty U_\infty^2 = f^*(\chi^*) = 0.19 + 2.75\chi^* + 4\chi^{*2} \tag{7}$$

The static pressure distribution (radially) inside a cylindrical shock[3,8] can be approximated as follows:

$$p_0/p_\infty = [p_0(0)/p_\infty][1 + j(\chi^{**})]$$

where $j(\chi^{**}) = 23\chi^{**}$, and

$$\chi^{**} = (R/d_N - \tfrac{1}{2})^4/(R_{sh}/d_N)^4 \tag{8}$$

Keuhn[9] gives the following correlation formula for the axial distribution of the pressure $p_0(0)$ (on the blast wave centerline):

$$p_0(0)/p_\infty = 0.85\, k(\gamma)/\Lambda + 0.55$$
$$\Lambda = C_{D_N}^{-1/2} M_\infty^{-2}(x/d_N - x_N/d_N) \tag{9}$$
$$k(\gamma) = 0.098(\gamma - 1)^{0.395} = 0.067 \text{ for } \gamma = 1.4$$

Equations (1–9) give the following embedded-Newtonian formulation of the pressure coefficient on a surface in the entropy wake generated by a blunt nose in air ($\gamma = 1.4$) at hypersonic speed ($M_\infty \to \infty$):

$$C_p = \frac{0.081\, C_{D_N}^{1/2}}{(x/d_N - x_N/d_N)}[1 + j(\chi^{**})] + C_{p_{\text{Newt}}} f^*(\chi^*) \tag{10}$$

For $\alpha = 0$ and small β and θ, Eq. (10) reduces in the static case ($q = 0$) to

$$C_p = \frac{0.081\, C_{D_N}^{1/2}(1 + 23\chi^{**})}{x/d_N(1 - x_N/x)} + C_{p_{\text{Newt}}} f^*(\chi^*) \tag{11}$$

The pressure distribution over blunted cones is correlated by the following formulation suggested by Cheng[10] and verified

† This should be a good assumption except for the flow region close to the shock.

by others[11,12]:

$$C_p/\theta_c^2 = F(\chi);\ \chi = \theta_c^2 C_{DN}^{-1/2}(x/d_N) \tag{12}$$

For small β and θ_F, when $23\chi^{**} \ll 1$, Eq. (11) can be written

$$C_p/\theta_F^2 = \frac{0.081}{\theta_F^2\, C_{DN}^{-1/2}\, x/d_N(1 - x_N/x)} + C_{p_{max}} f^*(\chi^*) \tag{13}$$

$$\chi^* = \beta^2 C_{DN}^{-1/2}\,(x/d_N)(1 - x_N/x)^{-1}$$

For a cone, $\beta = \theta_F = \theta_c$, and Eq. (13) becomes

$$\frac{C_p}{\theta_c^2} = \frac{0.081}{\chi(1 - x_N/x)} + C_{p_{max}} f^*(\chi^*) \tag{14}$$

$$\chi^* = \chi(1 - x_N/x)^{-1};\ \chi = \theta_c^2 C_{DN}^{-1/2}\,(x/d_N)$$

For regions not close to the nose, $(x_N/x)^2 \ll 1$, Eq. (14) approaches Eq. (12), with

$$F(\chi) = 0.081/\chi + C_{p_{max}} f^*(\chi) \tag{15}$$

Where the sharp cone pressure is approached on a blunted cone, the conical body surface is dictating the local shock shape. In general, then, the blast-wave-induced entropy wake on a cone will be different from that on a cylinder. One can, however, assume that the blast wave static pressure C_{p0} remains the same in both cases. Consequently, the cone pressure above this blast wave value, $C_p - C_{p0}$, is generated by the conical surface deflecting the entropy wake, i.e., $C_p - C_{p0} = C_{p_{max}} f^*(\chi)\theta_c^2$. Figure 2 shows the resulting shape of $C_{p_{max}} f^*(\chi)$ as given by Wagner's and Watson's correlation of cone pressures computed by the method of characteristics.[12] Thus for a blunted cone at angle of attack the pressure distribution is given by the following correlation formula, using the tangent-cone concept which Friberg[13] has shown to be a good representation as long as viscous effects are negligible:

$$C_p = \frac{0.081\ C_{DN}^{1/2}}{(x/d_N)\,(1 - x_N/x)} + 2\left(\frac{V_\perp}{U}\right)^2 f^*(\chi^*)$$

$$2f^*(\chi^*) = \begin{cases} 0.38 + 2.75\,\chi^* & :\ \chi^* \le 0.5 \\ 2 - 6.86(0.7 - \chi^*)^2 & :\ 0.5 < \chi^* < 0.7 \\ 2 & :\ \chi^* \ge 0.7 \end{cases}$$

$$\chi^* = (R/d_N - \tfrac{1}{2})^2/C_{DN}^{1/2}\,(x/d_N)(1 - (x_N/x) \tag{16}$$

Stability Derivatives

All static stability characteristics can be derived from the preceding equations. The unsteady characteristics are obtained as follows:

The effect of pitch rate q is obtained considering that

$$\partial/\partial(cq/U_\infty) = (U/U_\infty)^{-1}\partial/\partial(cq/U) \tag{17}$$

where

$$U/U_\infty = g^*(\chi^*)$$

The effect of time lag on the relative translatory position of the body element in the inviscid shear flow is

$$\Delta z = z(x,t) - z(x_N, t - \Delta t) \tag{18}$$

The time lag Δt occurring before a translation of the blast wave generator at x_0 has resulted in a translation of the shear flow at the body element (at x) is[7]

$$\Delta t = [(x - x_0)/U_\infty]/g^*(\chi^*) \tag{19}$$

For slow oscillations, $(cq/U_\infty)^2 \ll 1$, Δz can be written

$$\Delta z = \Delta z_{inst} + \Delta z(\Delta t)$$

$$\Delta z_{inst} = z(x,t) - z(x_0,t) = (x - x_0)\sin\alpha$$

$$\Delta z(\Delta t) = \dot z(x_0,t)\,\Delta t = (x - x_0)\dot z(x_0,t)/U_\infty g^*(\chi^*) \tag{20}$$

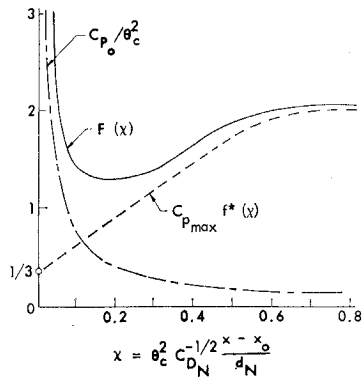

Fig. 2 Static pressure correlations.

For spherical nose bluntness, $x_0 = 0$, with the definitions given in Fig. 1.‡ The component $\Delta z(\Delta t)$ is neglected in heretofore available theories.

Seiff's data[3] give the following relation for the velocity ratio $g^* = U/U_\infty$ on a cylinder with hemisphere nose:

$$g^*(\chi^*) = 0.68 + 0.6\chi^{*1/2} \tag{21}$$

The g^*-profile linear in $\chi^{*1/2}$ would be stretched analogously to the stretching of the f^* profile, linear in χ^*, when going from the cylinder to the cone. With $f^* = 1$ and $g^* = 1$ for $\chi^* = 0.29$ on a cylinder and for $\chi^* = 0.59$ on a cone (using linear approximations), Eq. (21) becomes, for a cone

$$g^*(\chi^*) = 0.68 + 0.42\chi^{*1/2} \tag{22}$$

The linear f^* profile was valid up to $\chi^* = 0.5$; see Fig. 2 and Eq. (16). For $\chi^* = 0.5$, Eq. (22) gives $g^* = 0.977$. It appears well justified to approximate $g^*(\chi^*)$ as follows:

$$g^*(\chi^*) = \begin{cases} 0.68 + 0.42\chi^{*1/2} & :\ \chi^* < 0.5 \\ 1 & :\ \chi^* \ge 0.5 \end{cases} \tag{23}$$

For a rigid vehicle describing oscillations in pitch around c.g., Fig. 1 gives

$$z/d_N = z_{CG}/d_N + (x/d_N - x_{CG}/d_N)\sin\alpha$$

$$\dot z/d_N = \dot z_{CG}/d_N + (x/d_N - x_{CG}/d_N)\,(\cos\alpha)\dot\alpha \tag{24}$$

where $\dot\alpha = q$.

For small α and θ_c (with $\theta_c = \beta = \theta_F$), Eq. (16) defines the following static derivatives $(dC_p/d\alpha = C_{p\alpha} + \Delta^i C_p)_\alpha$:

$$C_{p\alpha} = \frac{0.081\ dC_{DN}/d\alpha}{2C_{DN}^{1/2}\,(x/d_N - x_N/d_N)} + 4\theta_c f^*(\chi^*) \times \left[1 + \left(\frac{\alpha}{\theta_c}\right)\sin\phi\right]\sin\phi \tag{25}$$

$$\Delta^i C_{p\alpha} = (\Delta^i C_{p\alpha})_{CDN} + (\Delta^i C_{p\alpha})_{zN}$$

$$(\Delta^i C_{p\alpha})_{CDN} = 4\theta_c^2(\partial f^*/\partial\chi^*)\chi^*[1 + (\alpha/\theta_c)\sin\phi]^2 \times \frac{(\Delta z/d_N) + [\frac{1}{2} + (x/d_N)\theta_c]\sin\phi}{(R/d_N)(R/d_N - \frac{1}{2})}\,\frac{d(\Delta z/d_N)}{d\alpha} \tag{26}$$

$$(\Delta^4 C_{p\alpha})_{zN} = -4\theta_c^2(\partial f^*/\partial\chi^*)\chi^*\,(1/2C_{DN})(dC_{DN}/d\alpha)$$

The corresponding unsteady derivatives are obtained when using Eqs. (17, 20, and 24) in conjunction with Eq. (16). For spherical nose bluntness, $(dc_{DN}/d\alpha) = 0$, the result is:

$$C_{pq} = 4\,\frac{f^*(\chi^*)}{g^*(\chi^*)}\left(\frac{d_N}{c}\right)\theta_c\left[1 + \left(\frac{\alpha}{\theta_c}\right)\sin\phi\right] \times \left[\left(\frac{x}{d_N} - \frac{x_{CG}}{d_N}\right) + \left(\frac{1}{2} + \frac{x}{d_N}\,\theta_c\right)\theta_c\right]\sin\phi \tag{27}$$

‡ For other nose geometries, $x_0 = 0$ can be assumed to be a good approximation.

$$\Delta^i C_p(t) = \frac{\partial \Delta^i C_p}{\partial(\Delta z/d_N)} \cdot \frac{\Delta z(\Delta t)}{d_N} =$$

$$(\Delta^i C_{p\alpha})_{C_{D_N}} \left[\frac{z_{CG}}{U_\infty} + \left(\frac{x_0}{c} - \frac{x_{CG}}{c} \right) \frac{\dot{\alpha} c}{U_\infty} \right] \Big/ g^*(\chi^*)$$

$$\Delta^i C_{p\dot{\alpha}} = \frac{\partial \Delta^i C_p}{\partial(c\dot{\alpha}/U_\infty)} = (\Delta^i C_{p\alpha})_{C_{D_N}} \left(\frac{x_0}{c} - \frac{x_{CG}}{c} \right) \Big/ g^*(\chi^*) \quad (28)$$

For hypersonic Mach numbers ($M_\infty \to \infty$) and spherical nose bluntness ($dC_{D_N}/d\alpha = 0$, $x_0 = 0$, $x_N = -d_N/2$), the preceding derivatives take the following form for a slender cone at moderate angles of attack (θ_c and α small):

$$C_{p\alpha} = 4\theta_c f^*(\chi^*) \left[1 + \left(\frac{\alpha}{\theta_c} \right) \sin\phi \right] \sin\phi$$

$$\Delta^i C_{p\alpha} = 4\theta_c \frac{\partial f^*(\chi^*)}{\partial \chi^*} \chi^* \left[1 + \left(\frac{\alpha}{\theta_c} \right) \sin\phi \right]^2 \times$$

$$\frac{x}{d_N} \theta_c \left[\frac{x}{d_N} \theta_c \left(\frac{\alpha}{\theta_c} \right) + \left(\frac{1}{2} + \frac{x}{d_N} \theta_c \right) \sin\phi \right] \Big/ \frac{R}{d_N} \left(\frac{R}{d_N} - \frac{1}{2} \right)$$

$$C_{p_q} = C_{p\alpha} \frac{d_N}{c} \left[\left(\frac{x}{d_N} - \frac{x_C G}{d_N} \right) + \left(\frac{1}{2} + \frac{x}{d_N} \theta_c \right) \theta_c \right] \Big/ g^*(\chi^*)$$

$$\Delta^i C_{p\dot{\alpha}} = -\Delta^i C_{p\alpha} \frac{x_{CG}}{c} \Big/ g^*(\chi^*)$$

$$\chi^* = 1.055 \left(\frac{R}{d_N} - \frac{1}{2} \right)^2 \Big/ \left(\frac{x}{d_N} + \frac{1}{2} \right) \quad (29)$$

R/d_N is given by Eq. (5) with $\Delta z/d_N = (x/d_N)\alpha$. At $\alpha = 0$, Eq. (29) simplifies to

$$C_{p\alpha} = 4\theta_c f^*(\chi^*) \sin\phi$$

$$\Delta^i C_{p\alpha} = 4.22\theta_c{}^3 \frac{\partial f^*(\chi^*)}{\partial \chi^*} \frac{x}{d_N} \sin\phi$$

$$\chi^* = 1.055\, \theta_c{}^2\, (x/d_N)/[1 + 1/(2\, x/d_N)] \quad (30)$$

The moment derivatives are obtained by integrating the pressure distribution given by Eq. (29) or Eq. (30) for the conical frustum, and adding the contribution from the nose tip itself, using modified Newtonian theory.

Finite Amplitude Oscillations

For finite amplitude oscillations in pitch, the effective stability derivatives $C_{\bar{m}_\theta}$ and $C_{\bar{m}_{\dot{\theta}}}$, corresponding to the linear measures of aerodynamic stiffness, $C_{m_\alpha} - (\omega c/U_\infty)^2 C_{m_{\ddot{\alpha}}}$, and damping, $C_{m_q} + C_{m_{\dot{\alpha}}}$, extracted from a dynamic wind tunnel test, are defined as follows[14]:

$$C_{\bar{m}_\theta} = \int_{\alpha_{\min}}^{\alpha_{\max}} [C_m - C_m(\alpha_{\min})] d\alpha \Big/ \int_{\alpha_{\min}}^{\alpha_{\max}} (\alpha - \alpha_{\min}) d\alpha \quad (31)$$

$$C_{\bar{m}_{\dot{\theta}}} = \int_{t_0}^{t_0+T} C_m d\theta \Big/ (c/U_\infty) \int_{t_0}^{t_0+T} \dot{\theta}^2 dt \quad (32)$$

where

$$\alpha = \alpha_0 + \theta$$

$$\alpha_{\max} = \alpha_0 + |\theta|,\ \alpha_{\min} = \alpha_0 - |\theta|$$

Equation (31) can be written in the following form, assuming antisymmetric characteristics, i.e., $C_m(-\alpha) = -C_m(\alpha)$:

$$C_{\bar{m}_\theta} = \frac{2}{(\alpha_{\max})^3/|\alpha_{\max}| - (\alpha_{\min})^3/|\alpha_{\min}|} \times$$

$$\left[\frac{\alpha_{\max}}{|\alpha_{\max}|} \int_0^{|\alpha_{\max}|} C_m d\alpha - \frac{\alpha_{\min}}{|\alpha_{\min}|} \int_0^{|\alpha_{\min}|} C_m d\alpha \right];\ |\alpha_0| < |\theta|$$

$$C_{\bar{m}_\theta} = \frac{2}{(\alpha_{\max} - \alpha_{\min})^2} \left[\frac{\alpha_{\max}}{|\alpha_{\max}|} \int_0^{|\alpha_{\max}|} C_m d\alpha - \right.$$

$$\left. \frac{\alpha_{\min}}{|\alpha_{\min}|} \int_0^{|\alpha_{\min}|} C_m d\alpha \right] + C_{m\alpha}(|\alpha_0|) - \frac{C_m(|\alpha_0|)}{|\theta|};\ |\alpha_0| > |\theta|$$

$$\int_0^{|\alpha_{\max}|} C_m d\alpha = \sum_1^N \Delta C_{m_n} [|\alpha_{\max}| - (\alpha_n + \alpha_{n-1})/2]$$

$$\int_0^{|\alpha_{\min}|} C_m d\alpha = \sum_1^M \Delta C_{m_n} [|\alpha_{\min}| - (\alpha_n + \alpha_{n-1})/2]$$

$$\Delta C_{m_n} = (\Delta C_{m_0})_n + (C_{m\alpha_{n-1}} + C_{m\alpha_n})(\alpha_n - {}_{n-1})/2 \quad (33)$$

For harmonic oscillations around $\alpha = \alpha_0$ (e.g., for $\theta = \Delta\theta \sin \omega t$), Eq. (32) becomes

$$C_{\bar{m}_{\dot{\theta}}} = \frac{1}{\pi \Delta\theta} \frac{1}{(\omega c/U_\infty)} \int_{\omega t_0}^{\omega t_0 + 2\pi} C_m \cos(\omega t) d(\omega t) \quad (34)$$

A slender blunted cone without flared aft body sections or trailing edge flaps will not experience any discontinuous aerodynamic characteristics, as are caused by separated flow[14] or shock-shock interactions.[15] Thus C_m can be described as a continuous function of angle-of-attack α. That is, $(\Delta C_{m_0})_n \equiv 0$ in Eq. (33), and Eq. (34) becomes

$$C_{\bar{m}_{\dot{\theta}}} = \frac{1}{\pi} \int_{\omega t_0}^{\omega t_0 + 2\pi} C_{m_{\dot{\theta}}}(|\alpha|) \cos^2(\omega t) d(\omega t) \quad (35)$$

$C_{m_{\dot{\theta}}}$ is the damping derivative for infinitesimal amplitude oscillations defined as a function of $|\alpha|$, $|\alpha| = |\alpha_0 + \Delta\theta \sin(\omega t)|$. According to the assumption of $C_m(-\alpha) = -C_m(\alpha)$, the damping derivative must be symmetric, i.e., $C_{m_{\dot{\theta}}}(-\alpha) = C_{m_{\dot{\theta}}}(\alpha) = C_{m_{\dot{\theta}}}(|\alpha|)$.

For oscillations around $\alpha_0 = 0$, the expressions for $C_{\bar{m}_\theta}$ and $C_{\bar{m}_\theta}$ become very much simpler:

$$C_{\bar{m}_\theta} = \frac{2C_m(\Delta\theta)}{\Delta\theta} -$$

$$\left\{ \sum_1^N [(C_{m\alpha_{n-1}} + C_{m\alpha_n})/2](\alpha_n{}^2 - \alpha_{n-1}{}^2) \right\} / (\Delta\theta)^2$$

$$= \frac{2C_m(N\Delta\alpha)}{N\Delta\alpha} -$$

$$\frac{1}{N^2} \sum_1^N [(2n-1)\, (C_{m\alpha_{n-}} + C_{m\alpha_n})/2] \quad (36)$$

where $\alpha_n - \alpha_{n-1} = \Delta\alpha = \Delta\theta/N$

$$C_{\bar{m}_{\dot{\theta}}} = \frac{2}{\pi} \int_{\omega t_0}^{\omega t_0 + \pi} C_{m_{\dot{\theta}}}(|\alpha|) \cos^2(\omega t) d(\omega t)$$

$$= \frac{4}{\pi} \int_0^{\pi/2} C_{m_{\dot{\theta}}}(\alpha) \cos^2\psi d\psi = \frac{2}{N} \sum_1^N C_{m_{\dot{\theta}}}(\alpha_n) \cos^2 \psi_n$$

$$\text{where } \alpha_n = \Delta\theta \sin\psi_n;\ \psi_n = [(n - \tfrac{1}{2})/N]\, \pi/2 \quad (37)$$

Discussion of Results

The analytic predictions of static and dynamic stability derivatives for a 5.6° cone at $\alpha = 0$ agree well with experi-

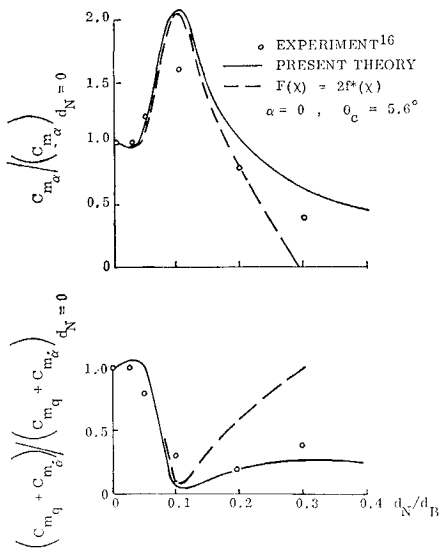

Fig. 3a Comparison between predicted and measured effect of nose bluntness for slender cones at $\alpha = 0$ and c.g. at $\Delta\bar{x}/l = 0.40$; $\theta_c = 5.6°$.

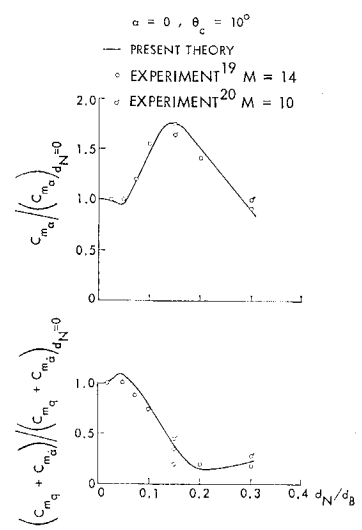

Fig. 3b Comparison between predicted and measured effect of nose bluntness for slender cones at $\alpha = 0$ and c.g. at $\Delta\bar{x}/l = 0.40$; $\theta_c = 10°$.

mental results[16] (Fig. 3a). For small nose bluntness, the effect of neglecting the blast wave pressure — $C_{p_0} = 0$, giving $F(\chi) = 2f^*(\chi)$ — is negligible, but at increasing nose bluntness the neglect produces increasingly poorer prediction of experimental results. It should be pointed out that in the formulation used for the effect of nose bluntness, viscous crossflow effects that are common to both pointed and blunted cones are eliminated from the comparison with the inviscid theory. The effect of nose bluntness on the viscous crossflow effect should be small as long as boundary-layer transition[17] or boundary-layer separation[18] does not occur on the (aft) body. The predictions of 10° cone data also agree well with experiments[19,20] at $M = 14$ and $M = 10$ (Fig. 3b).

The nonlinear effects of angle of attack measured by Walchner and Clay[16] are also predicted by the present theory, although the agreement could be better (Fig. 4). By ratioing, the blunted cone stability derivatives to the sharp cone data viscous (cross-flow) effects that are common to a blunted and a sharp cone are eliminated, permitting a realistic comparison with inviscid theoretical data. This certainly would be true for experiments with a thin turbulent boundary layer. Even for the relatively thicker laminar boundary layer, the

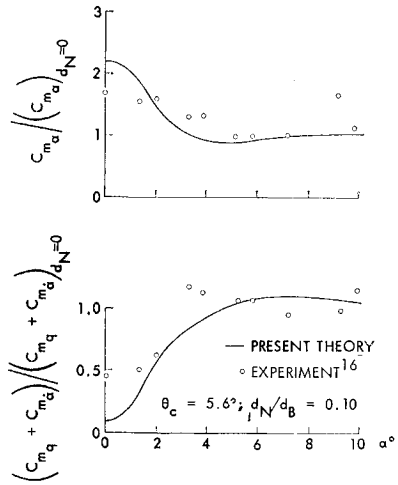

Fig. 4a Comparison between predicted and measured effects of nose bluntness for a 5.6° cone at various angles of attack with c.g. at $\Delta\bar{x}/l = 0.4$; $d_N/d_B = 0.10$.

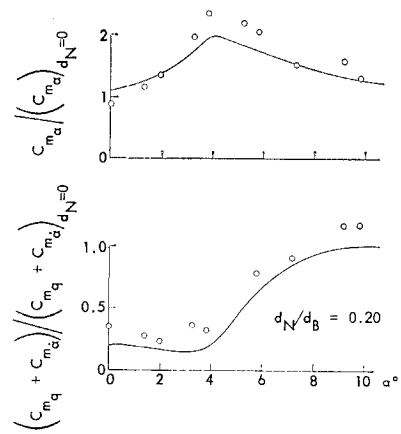

Fig. 4b Comparison between predicted and measured effect of nose bluntness for a 5.6° cone at various angles of attack with c.g. at $\Delta\bar{x}/l = 0.4$; $d_N/d_B = 0.20$.

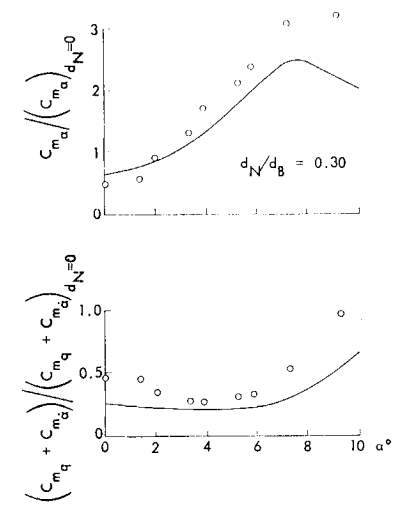

Fig. 4c Comparison between predicted and measured effects of nose bluntness for a 5.6° cone at various angles of attack with c.g. at $\Delta\bar{x}/l = 0.4$: $d_N/d_B = 0.30$.

viscous crossflow effects should not be very sensitive to nose bluntness unless boundary-layer transition occurs on the body.[17] Figure 5 shows that boundary-layer transition does not occur on the body at low angles of attack. However, at

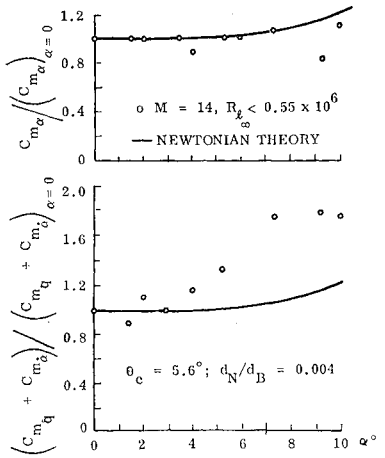

Fig. 5 Effect of boundary-layer transition on sharp cone damping at angle of attack with c.g. at $\Delta\bar{x}/l = 0.4$.

angles of attack above $\alpha = 4°$, boundary-layer transition takes place on the leeward side aft body of the sharp cone. The modest effect on static stability and large dynamically stabilizing effect are typical for a sharp cone where accelerated flow effects are large.[17] At increasing nose bluntness, the Reynolds number at the edge of the boundary layer on the conic frustum decreases, delaying the transition. (The decrease of boundary-layer edge Reynolds number has a greater delaying effect than the promoting effect of decreased boundary-layer edge Mach number.) As a consequence, a higher angle of attack will be required for the blunter cones before transition moves up on the body. The experimental data for high nose bluntness, therefore, may not be distorted by boundary-layer transition effects.§ Better agreement between theory and experiment is obtained (Figs. 6 and 7) if one eliminates the distorting effect of the boundary-layer transition occurring on the sharp cone, by using the stability derivative at $\alpha = 0$ as the normalizing unit for the nonlinear α effect.

When the blunt cone at angle of attack exposes its windward side to the entropy gradient effects, the expected trends of increased static and decreased dynamic stability result. Figure 7 shows the composition of the theoretical nonlinear characteristics. When the windward side moves out into the steep-gradient/high-energy portion of the entropy wake at increasing angles of attack, both local and gradient-induced forces increase. Statically, the local and induced derivatives, $C_{m\alpha}$ and $\Delta^i C_{m\alpha}$, add to each other, giving a steep increase of

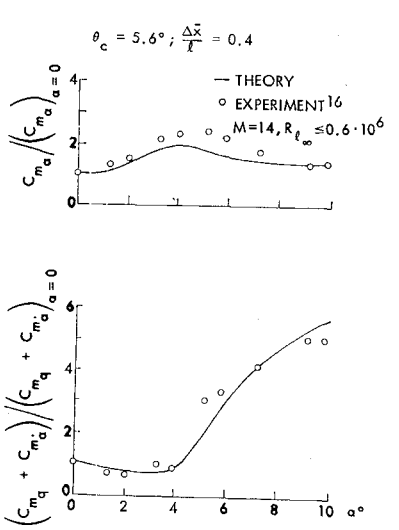

Fig. 6 Comparison between predicted and measured effects of angle of attack: $d_N/d_B = 0.20$.

§ So-called free-body vortices[11] cannot have been established on the model with the thick laminar boundary layer over the forebody.

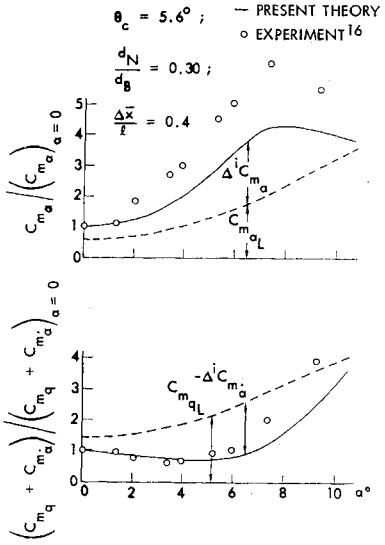

Fig. 7 Comparison between predicted and measured effects of angle of attack: $d_N/d_B = 0.30$.

static stability with increasing α. Dynamically, however, the induced derivative $\Delta^i C_{m\alpha}$ is undamping due to convective time lag effects[21]; as a result, the local damping derivative $C_{m_{q_L}}$ is reduced by $\Delta^i C_{m_{\dot\alpha}}$ and the total dynamic stability derivative $C_{m_q} + C_{m_{\dot\alpha}}$ is decreased with increasing α, the trend observed also experimentally (Fig. 7).

Thus far, theoretical stability derivatives for infinitesimally small amplitude pitch oscillations around trim angles of attack have been compared with measurements at finite amplitudes of 2° or less. This is justified. However, for large amplitude oscillations the concept of stability derivatives loses meaning when describing nonlinear aerodynamics. As was shown earlier, one can derive effective values, a "damping factor" $(C_{\bar{m}_{\dot\theta}})$, the $(C_{m_q} + C_{m_{\dot\alpha}})$ extracted from dynamic tests, and an "effective aerodynamic spring" $(C_{\bar{m}_\theta})$, which is the measured value $[C_{m\alpha} - (\omega c/U_\infty)^2 C_{m\dot\alpha}]$ in a dynamic test. Figure 8 shows how local and effective derivatives compare to each other, and Fig. 9 shows that theoretical predictions are in fair agreement with Ward's experimental data.[20] The underprediction of stability at high amplitudes is consistent with the underprediction of infinitesimal amplitude stability derivatives at large trim angles of attack (Fig. 7) and may indicate that viscous interaction at the nose starts to affect the over-all vehicle loads appreciably when the nose bluntness is large, $d_N/d_B \geq 0.30$. The experimental pressure distribution[13,22] indicates a substantial loss of (near) nose lift at high α, which

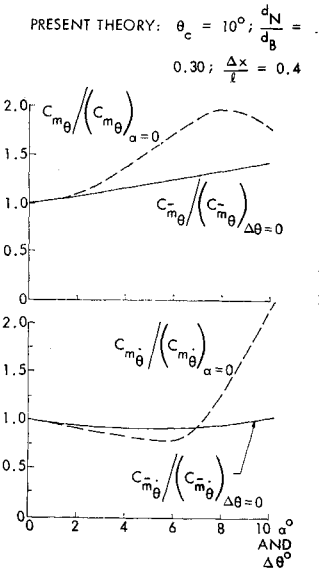

Fig. 8 Comparison between infinitesimal and finite amplitude stability derivative.

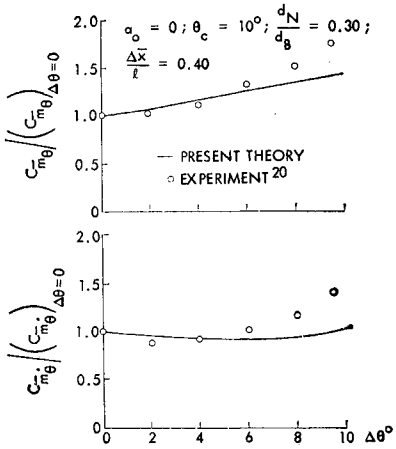

Fig. 9 Comparison between predicted and measured effects of oscillation amplitude.

would make the measured C_{m_α} more stable than predicted for inviscid flow. With negligible convective time lag effects for the near nose loads, the measured $(C_{m_q} + C_{m_{\dot\alpha}})$ would also be more stable—all in agreement with the observed deviations (Figs. 7 and 9).

It has been shown earlier that the presented analytical theory leads to universal scaling concepts for hypersonic nose-bluntness effects.[23] An example of this correlation is given in Fig. 10. It is undoubtedly true that most of the large nonlinear forces are generated on the windward side, which is moving out in the high-gradient, high-energy portion of the entropy wake, whereas the leeward side—"dipping down" to the zero-gradient, low-energy portion of the entropy wake—cannot contribute appreciable force change. Consequently, one may expect that using an average or effective cone to represent the windward side, thus defining an effective tangent cone angle at angle of attack, should provide some degree of scaling—including the combined effects of nose bluntness, cone angle, and angle of attack. If one assumes a constant value for the dynamic pressure ratio, $f^* = \text{const}$, the windward side effective tangent cone angle is

$$(\theta_c)_{\text{effective}} = \theta_c[1 + (8/3\pi)\alpha/\theta_c] \tag{38}$$

The corresponding effective scaling parameters is

$$\bar{\chi}_l = \chi_l[1 + (8/3\pi)\alpha/\theta_c] \tag{39}$$

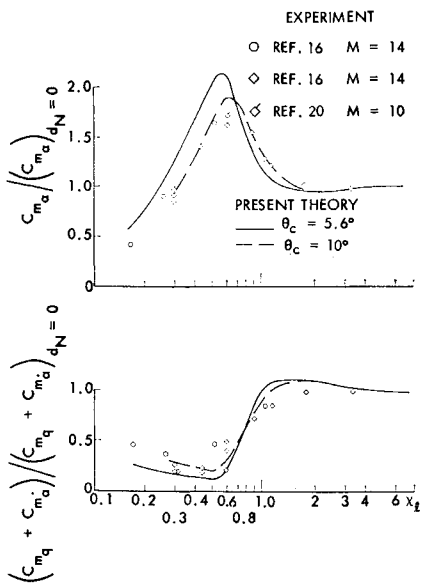

Fig. 10 Scaling of nose-bluntness effects at $\alpha = 0$ and c.g. at $\Delta\bar{x}/l = 0.40$.

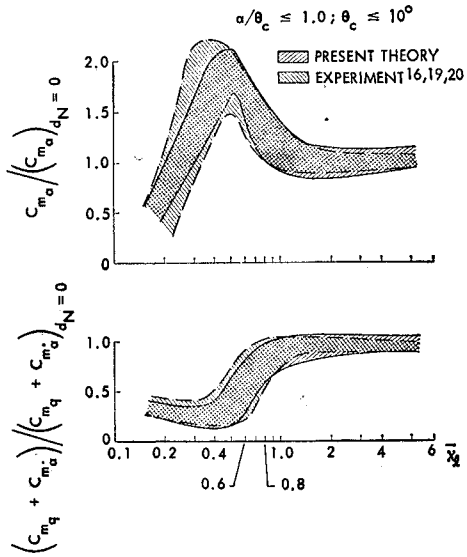

Fig. 11 Approximate scaling of effects of nose bluntness, cone angle, and angle of attack for c.g. at $\Delta\bar{x}/l = 0.40$.

where χ_l is the scaling parameter derived previously[23] for $\alpha = 0$,

$$\chi_l = (\tan\theta_c/2)/(d_N/d_B)C_{D_N}{}^{1/2} \tag{40}$$

Figure 11 shows this approximate scaling to work for cone half-angles up to 10° and angles of attack up to cone half-angle magnitudes. The agreement between theoretical and experimental data is rather good.¶ It is true that the data bands are rather broad, as could be expected because of the rather crude approximations used in defining $\bar{\chi}_l$. It is also true, however, that in many instances the accuracy is sufficient for preliminary design purposes. When better accuracy is needed for a specific configuration, the analytic theory presented here will supply the needed answer.

References

[1] Hayes, W. D., and Probstein, R. F., *Hypersonic Flow Theory*, Academic Press, New York, 1959.

[2] Seiff, A. and Whiting, E. E., "The Effects of the Bow Shock Wave on the Stability of Blunt-Nosed Slender Bodies," TMX-377, Sept. 1960, NASA.

[3] Seiff, A. and Whiting, E. E., "Calculation of Flow Fields from Bow-Wave Profiles for the Downstream Region of Blunt-Nosed Circular Cylinders in Axial Hypersonic Flight," TND-1147, Nov. 1961, NASA.

[4] Seiff, A., "Secondary Flow-Fields Embedded in Hypersonic Shock Layers," TND-1304, May 1962, NASA.

[5] Gravalos, F. G., Edfelt, I. H., and Emmons, H. W., "The Supersonic Flow About a Blunt Body of Revolution for Gases at Chemical Equilibrium," *Proceedings of the IX International Astronautical Congress*, Amsterdam, 1958, pp. 312–332.

[6] Seiff, A. and Whiting, E. E., "A Correlation Study of the Bow-Wave Profiles of Blunt Bodies," TND-1148, Feb. 1962, NASA.

[7] Ericsson, L. E., "Unsteady Aerodynamics of an Ablating Flared Body of Revolution Including Effect of Entropy Gradient," *AIAA Journal*, Vol. 6, No. 12, Dec. 1968, pp. 2395–2401.

[8] Lin, S. C., "Cylindrical Shock Waves Produced by Instantaneous Energy Release," *Journal of Applied Physics*, Vol. 25, No. 1, Jan. 1954, pp. 54–57.

[9] Keuhn, Donald M., "Experimental and Theoretical Pressures on Blunt Cylinders for Equilibrium and Nonequilibrium Air at Hypersonic Speeds," TND-1979, 1963, NASA.

[10] Cheng, H. H., "Hypersonic Flow With Combined Leading Edge Bluntness and Boundary Layer Displacement Effect," Rept. AF-1285-A-4, Contract W-2653(00), Aug. 1960, Cornell Aeronautical Lab., Buffalo, N.Y.

¶ Similar results, of course, can be expected for the effective stability derivatives at finite oscillation amplitudes.

[11] Griffith, B. J. and Lewis, C. H., "A Study of Laminar Heat Transfer to Spherically Blunted Cones and Hemisphere-Cylinders at Hypersonic Conditions," AEDC-TDR-63-102, June 1963, Arnold Engineering Development Center.

[12] Wagner, R. D., Jr. and Watson, R., "Induced Pressures and Shock Shapes on Blunt Cones in Hypersonic Flow," TND-2182, March 1964, NASA.

[13] Friberg, E. G., "Pressure Distribution on a 5.6° Blunt Cone at Mach 14," ARL 68-02,08, Nov. 1968, Aerospace Research Lab.

[14] Ericsson, L. E., "Separated Flow Effects on the Static and Dynamic Stability of Blunt Nosed Cylinder Flare Bodies," LMSC-667991, Contract NAS 8-5338, Dec. 1965, Lockheed Missiles & Space Co., Sunnyvale, Calif.

[15] Ericsson, L. E. and Reding, J. P., "Dynamic Stability Problems Associated with Flare Stabilizers and Flap Controls," *Journal of Spacecraft and Rockets*, Vol. 7, No. 2, Feb. 1970, pp. 132–137.

[16] Walchner, O. and Clay, J. T., "Nose Bluntness Effects on the Stability Derivatives of Cones in Hypersonic Flow, *Transactions of the Second Technical Workshop on Dynamic Stability Testing*, Vol. 1, Paper 8, April 1965, Arnold Engineering Development Center, Arnold Air Force Station, Tenn.

[17] Ericsson, L. E., "Effect of Boundary Layer Transition on Vehicle Dynamics," *Journal of Spacecraft and Rockets*, Vol. 6, No. 12, Dec. 1969, pp. 1404–1409.

[18] Rainbird, W. J., "Turbulent Boundary-Layer Growth and Separation on a Yawed Cone," *AIAA Journal*, Vol. 6, No. 12, Dec. 1968, pp. 2410–2416.

[19] Clay, J. T., "Nose Bluntness, Cone Angle, and Mach Number Effects on the Stability Derivatives of Slender Cones," ARL 67-0185, Sept. 1967, Aerospace Research Lab.

[20] Ward, L. K., Jr. and Uselton, B. L., "Dynamic Stability Results for Sharp and Blunted 10-deg Cones at Hypersonic Speeds," *Transactions of the 3rd Technical Workshop on Dynamic Stability Problems*, Vol. III, Paper 2, Nov. 1968, NASA.

[21] Ericsson, L. E. and Scholnick, I. M., "Effect of Nose Bluntness on the Hypersonic Unsteady Aerodynamics of Flared and Conical Bodies of Revolution," *Journal of Spacecraft and Rockets*, Vol. 6, No. 3, March 1969, pp. 321–324.

[22] Friberg, E. G. and Walchner, O., "Pressure Correlation for Blunted Slender Cones," *AIAA Journal*, Vol. 7, No. 8, Aug. 1969, pp. 1618–1619.

[23] Ericsson, L. E., "Universal Scaling Laws for Nose Bluntness Effects on Hypersonic Unsteady Aerodynamics," *AIAA Journal*, Vol. 7, No. 12, Dec. 1969, pp. 2222–2227.

FEBRUARY 1971 AIAA JOURNAL VOL. 9, NO. 2

Interaction of Sonic Transverse Jets with Supersonic External Flows

C. C. Lee* and B. F. Barfield†
University of Alabama, University, Ala.

This paper presents a theoretical analysis for the determination of the two-dimensional flowfield in the vicinity of the injection port of a secondary sonic jet normal to a supersonic external stream. The solution is valid for flows in which the boundary layer is nonexistent and mixing effects can be neglected. The gas is assumed to be perfect and inviscid. The method of characteristics was employed in the determination of the jet flowfield, and the time-dependent finite-difference method was employed to determine the external flowfield. The key to the over-all solution lies in coupling the flowfields through the jet boundary. This is accomplished by constraining the static pressure to be continuous across the jet boundary. The coupling technique developed herein has proven successful, and the entire theory, through the use of the coupling technique, has been formulated into a computer program. Extensive calculations have been carried out to study the effect of freestream Mach number, jet total pressure and ratio of specific heats on penetration, shock stand-off distance, and upstream pressure distribution.

Introduction

WHEN a secondary jet issues laterally into a supersonic stream, the interaction between the two streams creates a high pressure region on the wall surface in front of the jet port. The resulting force due to this high pressure can be several times larger than the thrust of the jet alone. Therefore, the interaction mechanism presents itself as a very useful technique for the vector control of high-speed flight vehicles. In addition, the secondary jet device has several other advantages over the conventionally used fins, such as 1) eliminating the aerodynamic heating problem on the control surfaces, 2) being effective at all altitudes, and 3) possibility of a weight saving design. In order to employ the jet control properly, prediction of shock behavior, static pressure distribution on the surface, and all the flow properties in the neighborhood of the jet exit is necessary. In the past few years, an intensive effort has been devoted to this problem by many research groups. However, this effort has been primarily experimental in nature with the goal of obtaining fundamental information, similarity rule,[1–8] drawing analogies,[9–12] developing simple analytic models[13–17] (discussion of previous work as presented in Ref. 18). To date, no analytical method has been published that presents a direct approach for the determination of shock behavior or other flow properties. The purpose of this paper is to present the result of a theoretical approach to this problem. This approach is based on the inviscid flow assumption, i.e., nonexistence of boundary layer. The flow model is depicted in Fig. 1. The solution is developed by coupling the jet flow region, in which the method of characteristics is applicable, to the external flow region determined by the application of the time-dependent finite-difference method. This flow model may seem unrealis-

Received February 16, 1970; revision received June 29, 1970. This research was partially supported by the Bureau of Engineering Research, University of Alabama, University, Ala.

* Research Associate; now Group Engineer, Propulsion, at McDonnell Aircraft, St. Louis, Mo.

† Associate Professor, Department of Mechanical Systems Engineering. Member AIAA.